buildings

MDPI

Article

Axial Compression Behavior of Novel Latticed Columns with CFST Tubes and Corrugated Steel Plates for Industrial Structures

Xuan Zhao [1,2], Ningning Zhang [2,*], Zhaohui Hu [1,2], Xian Li [2], Ying Nie [1] and Jun Liu [3,4]

[1] CISDI Group Co., Ltd., Chongqing 400013, China; xuan.zhao@cisdi.com.cn (X.Z.); zhaohui.hu@cisdi.com.cn (Z.H.); ying.nie@cisidi.com.cn (Y.N.)
[2] School of Mechanics and Civil Engineering, China University of Mining and Technology, Xuzhou 221000, China; lixian@cumt.edu.cn
[3] School of Civil Engineering, Xi'an University of Architecture and Technology, Xi'an 710055, China; liujun@xauat.edu.cn
[4] XAUAT Engineering Technology Co., Ltd., Xi'an 710055, China
* Correspondence: tb23030010a41@cumt.edu.cn

Abstract: Metallurgical industrial buildings, particularly those over 10 years old, frequently experience increased vibrations in their latticed columns due to prolonged dynamic loads from cranes, affecting both structural safety and usability. To enhance the strength and stiffness of these structures in a cost-effective way, a novel composite latticed column made from concrete-filled steel tubes and corrugated steel plates is proposed. An analytical study on its axial compression behavior has also been conducted. The analytical parameters included the yield strength of steel tube and compressive strength of concrete, the waveform of corrugated steel plate, as well as the thickness, yield strength, and configuration of steel lacing tubes. Results show that compared to specimens with C30 concrete, the bearing capacity and initial axial stiffness of specimens with C50 concrete can increase by 35% and 33%, respectively. Compared with the steel specimen with yield strength of 235 MPa, the peak bearing capacity of the steel specimen with yield strength of 400 MPa can be increased by 28%. Additionally, increasing the wave height reduces the concrete cross section, resulting in a decrease in axial stiffness and ductility. Compared to specimens with horizontal lacing tubes, those with diagonal lacing tubes exhibit increases in ductility and axial stiffness of 33% and 12%, respectively. Therefore, diagonal lacing tubes should be considered for the optimal axial compression behavior of latticed columns. Furthermore, a model for predicting the axial compression bearing capacity of latticed columns with CFST tubes and corrugated steel plates was proposed.

Keywords: latticed column; concrete filled steel tube; corrugated steel plate; axial compression behavior; numerical simulation

check for updates

Academic Editor: Eric M. Lui

Received: 26 November 2024
Revised: 20 December 2024
Accepted: 24 December 2024
Published: 26 December 2024

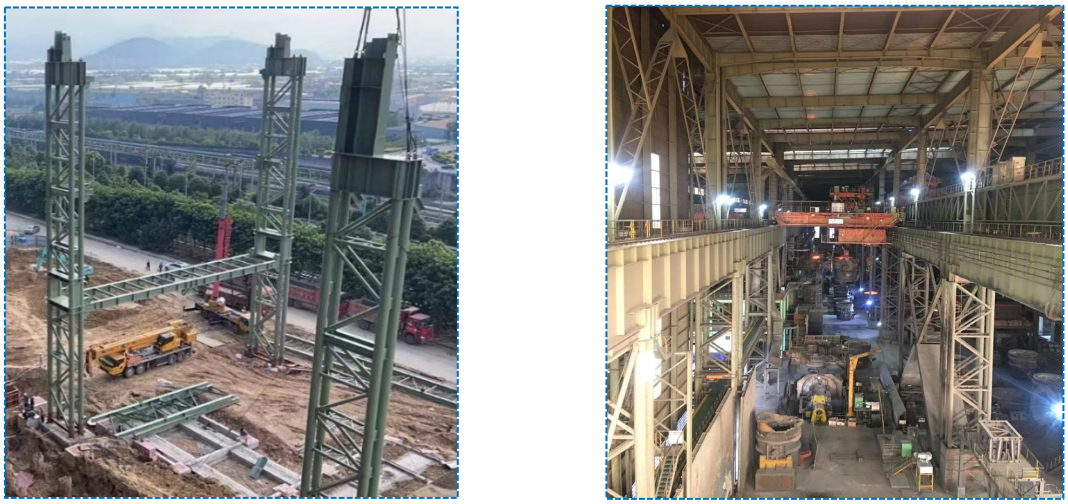
Citation: Zhao, X.; Zhang, N.; Hu, Z.; Li, X.; Nie, Y.; Liu, J. Axial Compression Behavior of Novel Latticed Columns with CFST Tubes and Corrugated Steel Plates for Industrial Structures. *Buildings* **2025**, *15*, 42. https://doi.org/10.3390/buildings15010042

Copyright: © 2024 by the authors. Licensee MDPI, Basel, Switzerland. This article is an open access article distributed under the terms and conditions of the Creative Commons Attribution (CC BY) license (https://creativecommons.org/licenses/by/4.0/).

1. Introduction

Concrete filled steel tubes (CFSTs) are extensively utilized in high-rise buildings, industrial structures, and bridge engineering due to their exceptional mechanical properties [1]. The CFST latticed column, integrated with CFST limb columns via steel tube braces, exhibits superior section inertia and bending stiffness compared to a single-limb CFST tube. This configuration ensures that the compressive bearing capacity of CFST can be fully leveraged even under the condition of significant eccentricity [2,3]. Recently, numerous researchers have conducted comprehensive research on the eccentric compression, axial compression, and hysteretic behavior of CFST latticed columns [4,5], laying a robust foundation for the advancement of design and practical applications related to CFST latticed columns [6–10].

CFST latticed columns are frequently employed in metallurgical industrial buildings characterized by their high story height and heavy load, as illustrated in Figure 1. To accommodate crane operations, the two CFST column limbs of the latticed column in such industrial buildings are typically positioned closely together along the crane's direction, while the distance between the limbs is widened in the perpendicular direction. As depicted in Figure 1b, the center-to-center distances between the limb columns in these two orientations are 1 m and 3 m, respectively. Field investigations have shown that many industrial buildings experience increased vibrations in their latticed columns due to prolonged exposure to dynamic loads from cranes, particularly those that have been in service for more than 10 years, seriously affecting the normal use and safety of the structure [11]. Consequently, it is imperative to explore economical and reasonably feasible methods to augment the lateral stiffness and lateral bearing capacity of the latticed columns.



(**a**) Industrial buildings under construction (**b**) Industrial building in operation

Figure 1. Scene photos of industrial buildings. (Courtesy of Jun Liu).

In response to this issue, in this paper a novel composite structural column leveraging the benefits of high out-of-plane stiffness and substantial shear strength inherent in corrugated steel plates was proposed, as depicted in Figure 2. Taking into account the specific cross-sectional characteristics of industrial building latticed columns, this innovative composite column connects two closely spaced column limbs using two corrugated steel plates and infilled concrete, whereas the limbs positioned farther apart remain joined by lacing tubes. This configuration not only accommodates the spatial needs of industrial buildings but also substantially elevates the load-bearing capacity and lateral stiffness of CFST latticed columns. The corrugated steel plates, distinguished by their distinctive geometry and superior mechanical properties, enhance the shear strength and buckling resistance of plates even with significant width-to-thickness ratios [12]. Therefore, corrugated panels have been widely used in various engineering fields, such as aviation, aerospace, automotive, and civil engineering [13]. In addition, the corrugated steel plates effectually confine concrete core [14–17]. Existing research attests to the corrugated steel plates' superior shear resistance [18,19], torsional resistance [20,21], and bending performance [22,23], highlighting their enhanced flexural capacity and ductility [24]. Some scholars also have studied the modeling and optimization of corrugated steel plates [13,25].

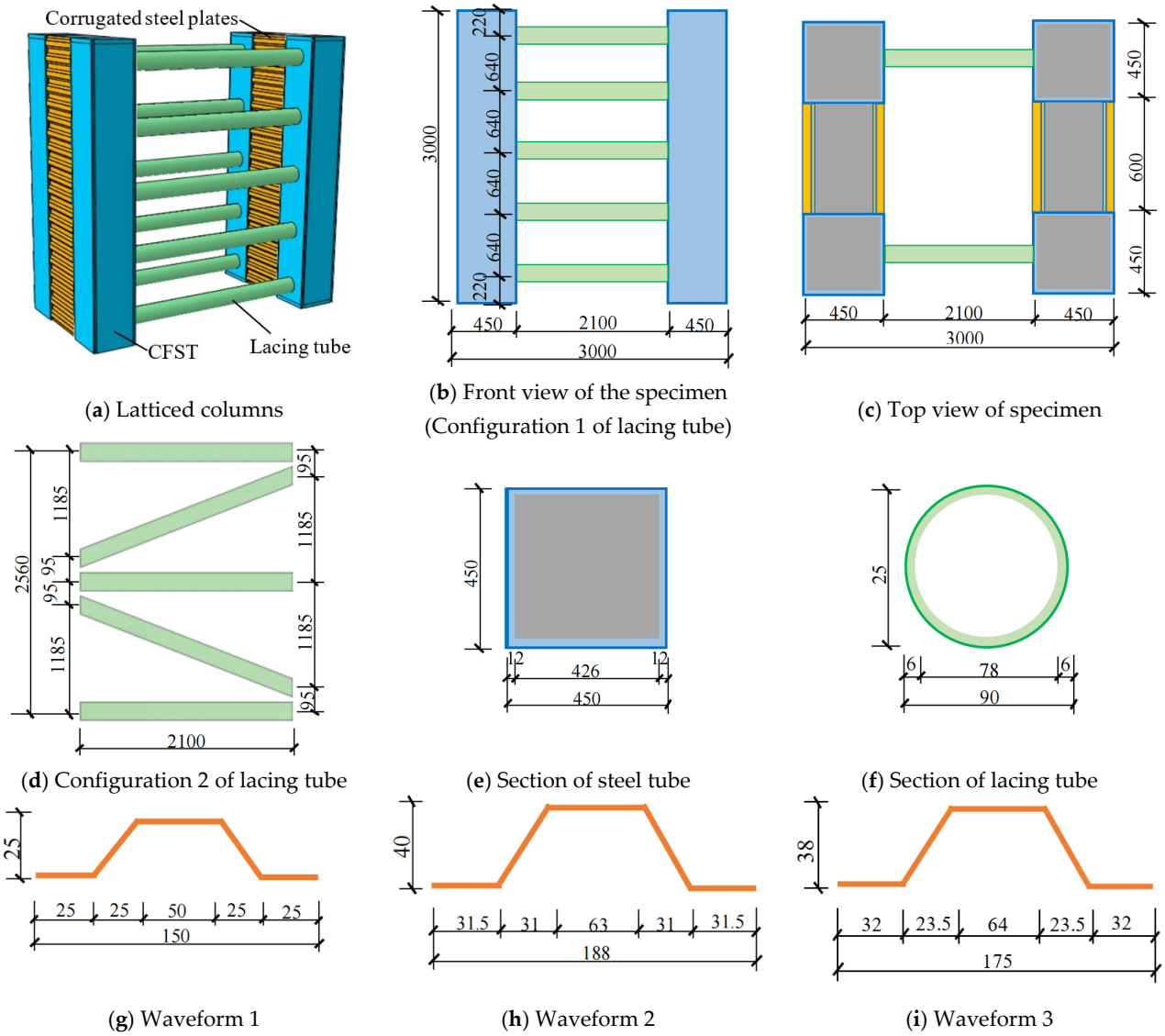


Figure 2. Specimen schematic and size (unit: mm).

To study the axial compressive performance of the proposed latticed column, the finite element software ABAQUS 2020 [26] was used to carry out refined simulation and parameter analysis. This study investigates the impacts of various parameters, such as the strength of the steel tube and concrete, the waveform of the corrugated plates, and the thickness, strength, and configuration of the lacing tubes. Additionally, a model for estimating the axial compression performance of the columns was developed based on the finite element method (FEM) results.

2. Finite Element (FE) Model

2.1. Specimen Design

Using a four-limb latticed column of a metallurgical industrial plant as the prototype, the proposed latticed column was designed, and the dimensions of the column were set at a height of 3000 mm, length of 3000 mm, and width of 1500 mm to better study the axial compression performance. The latticed column consists of four CFST columns that encase corrugated steel plates filled with concrete and steel lacing tubes. The steel tube has a width of 450 mm and a thickness of 12 mm. Two concrete-filled corrugated steel plates

are placed between two steel tubes that are 2100 mm apart on the same side, and each plate has a width of 600 mm. The steel lacing tubes are arranged between the steel tubes.

To investigate the axial compression behavior of the CFST latticed column under axial compressive loads, this paper presents the design of 13 latticed column specimens with varying parameters. The design parameters include the yield strength of steel tube (f_y), the compressive strength of concrete (f_c), lacing thickness (t_l), the yield strength of lacing tube (f_L), lacing configuration, and the waveform of the corrugated steel plate. Detailed parameters are provided in Tables 1 and 2. Notably, specimen T1 serves as a typical example, making it representative and facilitating analysis and comparison in subsequent research.

Table 1. Size, strength, and configuration information of specimens.

No.	Specimen	Yield Strength of Steel Tube f_y (MPa)	Compressive Strength of Concrete f_c (MPa)	Thickness of Lacing Tube t_l (mm)	Yield Strength of Lacing Tube f_L (MPa)	Configuration of Lacing Tube	Waveform of Corrugated Plate
1	T1	235	30	6	355	Configuration 1	Waveform 1
2	H1	355	30	6	355	Configuration 1	waveform 1
3	H2	400	30	6	355	Configuration 1	waveform 1
4	C1	235	40	6	355	Configuration 1	waveform 1
5	C2	235	50	6	355	Configuration 1	waveform 1
6	LT1	235	30	4	355	Configuration 1	waveform 1
7	LT2	235	30	5	355	Configuration 1	waveform 1
8	LT3	235	30	7	355	Configuration 1	waveform 1
9	LQ1	235	30	6	235	Configuration 1	waveform 1
10	LQ2	235	30	6	400	Configuration 1	waveform 1
11	LX1	235	30	6	355	Configuration 2	waveform 1
12	B1	235	30	6	355	Configuration 1	waveform 2
13	B2	235	30	6	355	Configuration 1	waveform 3

Note: The configurations of lacing tube are shown in Figure 2b,d, and the waveform of the corrugated plate are shown in Figure 2g–i.

Table 2. Size information of specimen T1.

	Steel Tube $B_s \times t_s$ (mm)	Wide of Corrugated Plate B_c (mm)	Thickness of Corrugated Plate t_c (mm)	Length of Lacing Tube L (mm)
T1	450 × 12	600	1.2	2100

Note: B_s represents the wide of the steel tube, t_s represents the thickness of the steel tube, t_c represents the thickness of corrugated plate, and L represents the length of the lacing tube.

2.2. Modeling Method and Boundary Conditions

The FE models of the latticed column are developed by finite element analysis software ABAQUS, as shown in Figure 3. The 8-node linear reduced integration solid elements are adopted for the steel tubes, concrete, corrugated steel plates, and lacing tubes. Through the mesh sensitivity analysis, the size of the global mesh is set to 40 mm. Additionally, surface-to-surface contact is employed for the interactions between the concrete and the steel tube, as well as between the concrete and the corrugated steel plate, and the tangential friction coefficient is set to 0.2. Tie contact is adopted for steel tubes with corrugated plates and lacing tubes. It should be mentioned that due to the Tie connection between the lacing tube and steel tube, the deformation is coordinated, so the coupling of the meshes of the two is not considered. Coupling points are set at the top and bottom of the column, and boundary conditions and displacement loading are applied to the coupling points. The boundary conditions at the bottom of the latticed column are set as U1 = U2 = U3 = UR1 = UR2 = 0. For the top of the latticed column, the conditions are set to U2 = −30 mm, while U1 = U3 = UR1 = UR2 = 0.

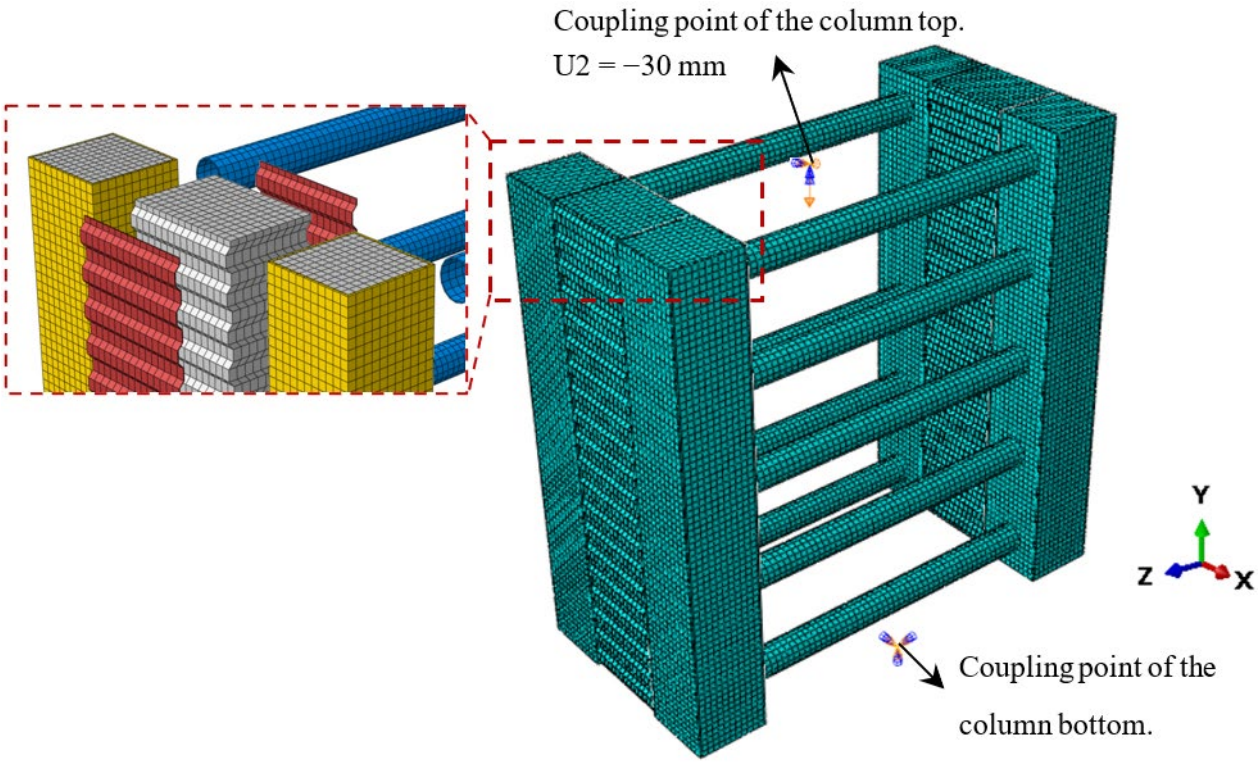


Figure 3. Mesh and boundary conditions of the latticed columns.

2.3. Material Constitutive Model

2.3.1. Concrete

The stress–strain relationship proposed by Han (2016) is used for the core concrete [1]. This relationship considers the constraint effect, as shown in Figure 4.

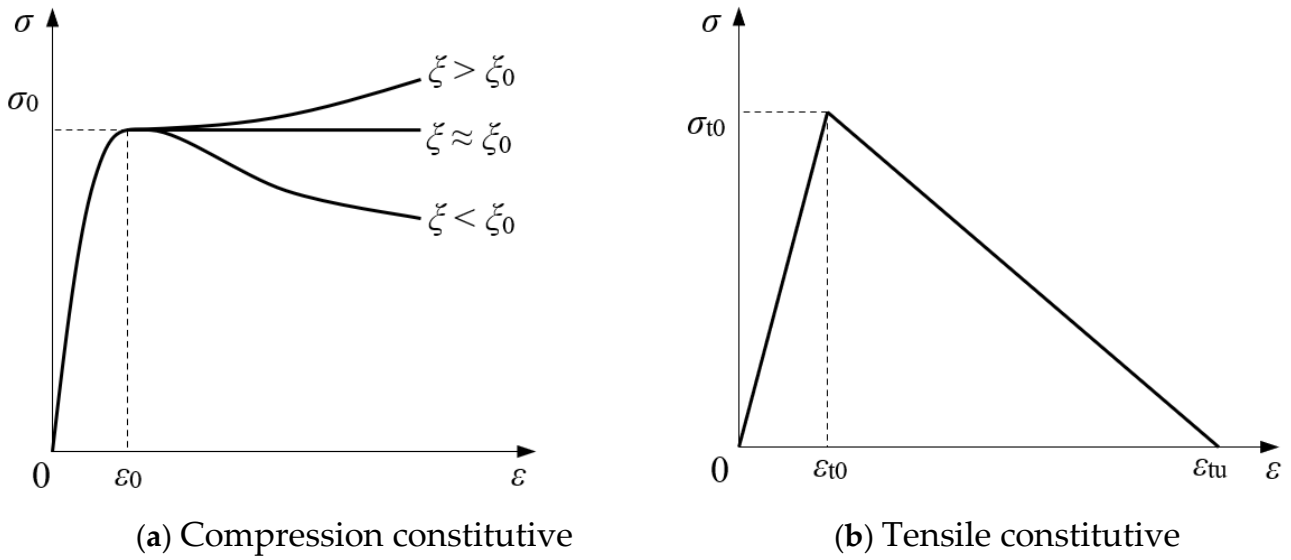


Figure 4. Stress–strain curves of concrete [23].

2.3.2. Steel

The constitutive relationship proposed by Esmaeily et al. [27] is used for steel, which can be seen in the black line in Figure 5a. Considering the steel fracture, the damage evolution of steel is supplemented to the constitutive relationship. According to Refs. [28,29], the path of equivalent plastic damage strain and stress triaxiality η is shown in Figure 5b.

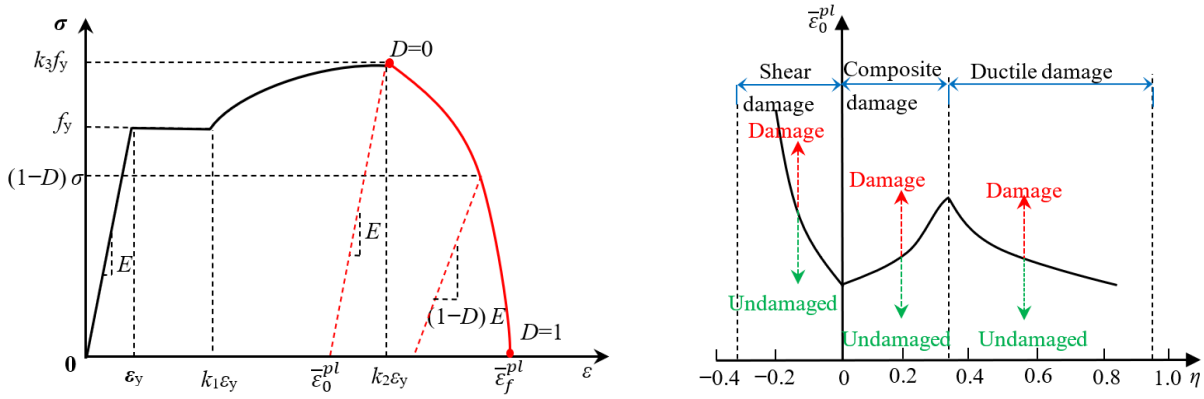
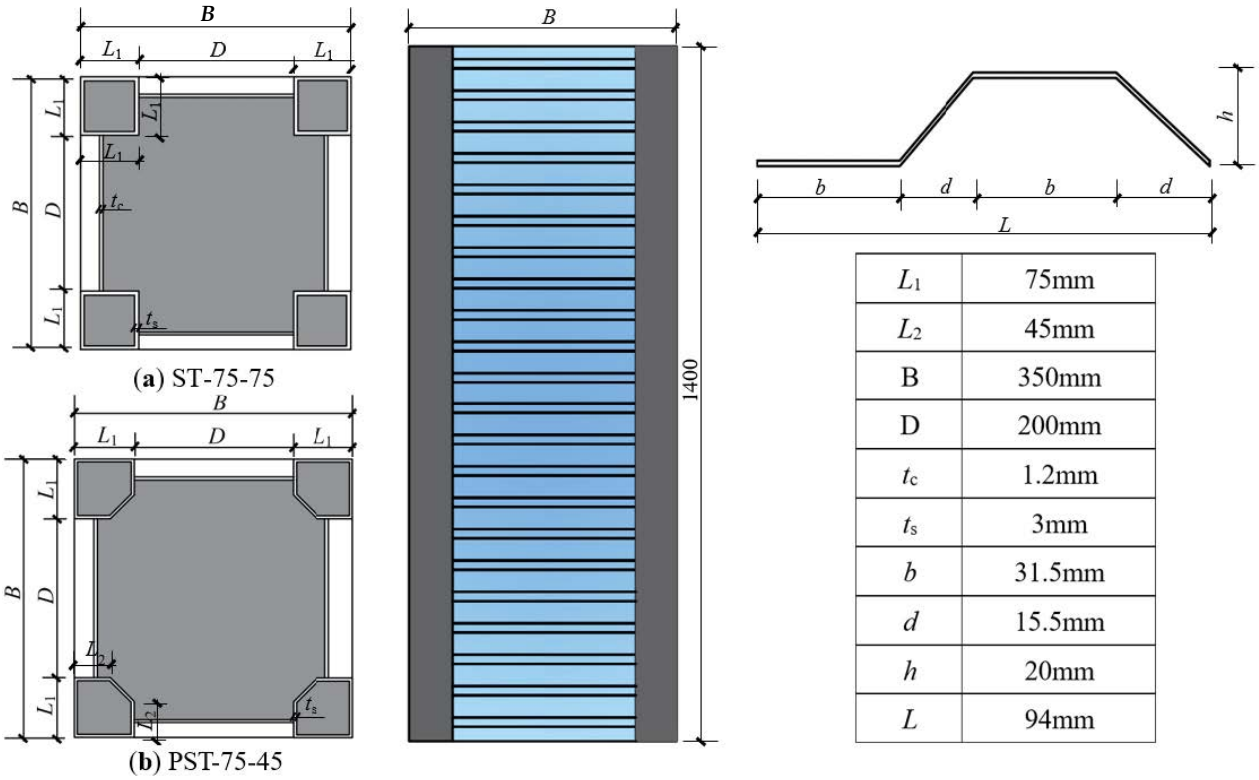


Figure 5. Constitutive relationship of steel [23]. (**a**) Stress–strain relation curve of steel; (**b**) Stress triaxiality and equivalent plastic damage strain path of steel.

3. Validation of the FE Model

Axial compression tests on polygonal concrete columns composed of CFST columns and corrugated steel plates [30] were chosen to verify the rationality of the modeling method and material constitutive models. The specimen size is shown in Figure 6.

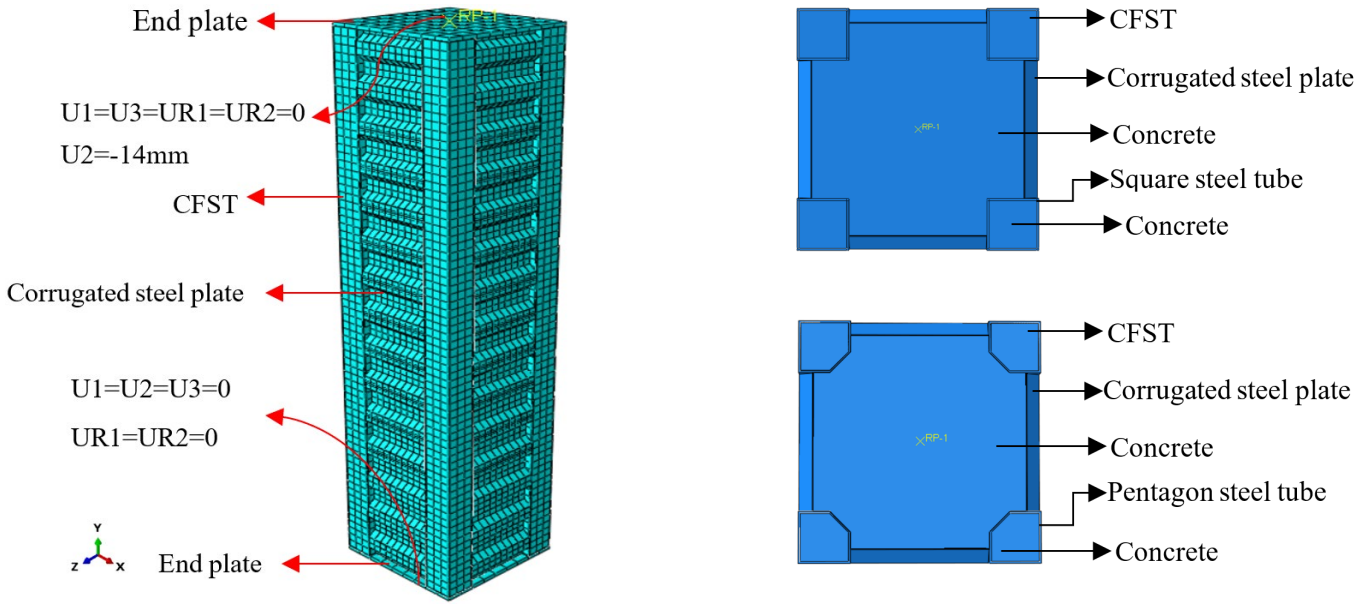


L_1	75mm
L_2	45mm
B	350mm
D	200mm
t_c	1.2mm
t_s	3mm
b	31.5mm
d	15.5mm
h	20mm
L	94mm

Figure 6. Size of the column [30].

The FE model of the polygonal steel tube and corrugated steel plate concrete column specimens (specimen ST-75-75 and specimen PST-75-45) [30] was established by ABAQUS, as shown in Figure 7. In this model, the 8-node linear reduced integration solid elements are used for the steel tube, corrugated steel plate, concrete, and the end plates. The mesh size is set to 50 mm, while the refined area size is set to 20 mm. Surface-to-surface contact is employed for the interactions between the concrete and the steel tube, as well as between the concrete and the corrugated steel plate, and the tangential friction coefficient is set to

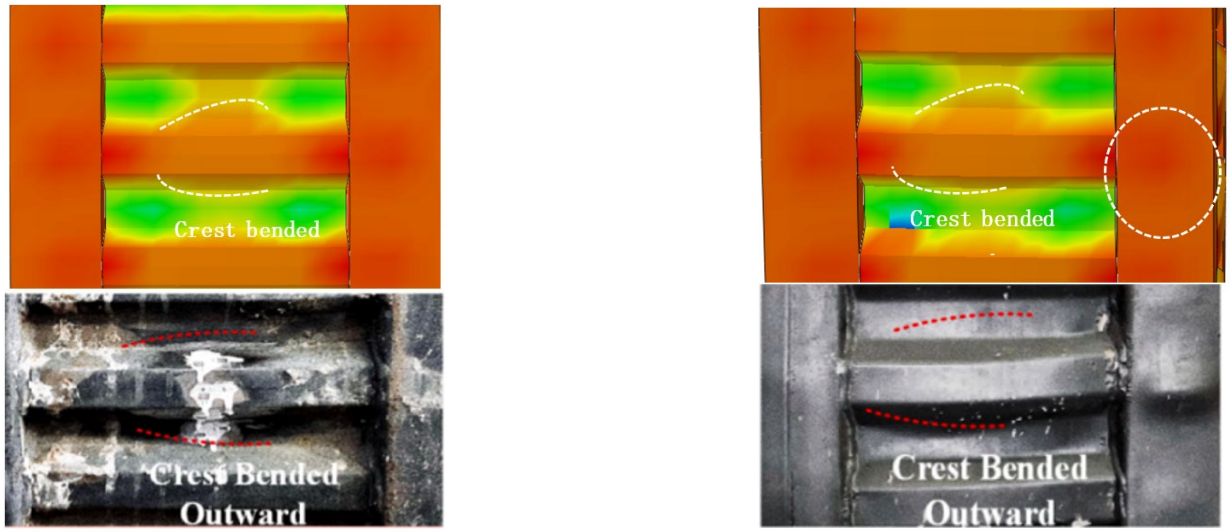
0.45. Tie contact is adopted between the steel tube, lacing tubes, corrugated steel plate, concrete, and the end plates. The boundary condition of the roof is set to U1 = U3 = UR1 = UR2 = 0, and the vertical displacement is set to −14 mm. The boundary condition of the bottom plate is set as U1 = U2 = U3 = UR1 = UR2 = 0 to simulate the column bottom constraint, and only the rotation caused by axial compression is allowed.



(**a**) Mesh and boundary conditions (**b**) Section of the specimen

Figure 7. FE model of columns.

Figure 8 shows the deformation result of the column under axial compression load of numerical simulation and experiment. It can be seen that local outward buckling occurs in the middle of the corrugated plate, and local buckling occurs in the middle of the PST-75-45 steel tube. The failure modes of FE model are consistent with the experimental phenomenon.



(**a**) ST-75-75 (**b**) PST-75-45

Figure 8. Comparison of failure phenomenon between test and FE model.

Figure 9 shows the load–displacement curves of the two specimens under axial compression load obtained by the test and numerical simulation. The trend of the curves is basically the same. The errors of the peak bearing capacity of the specimen ST-75-75 and the specimen PST-75-45 between the FE model and the experiment are 1.6% and 2.8%, respectively. This shows that the failure phenomenon of the FE model is in good agreement with experimental phenomenon.

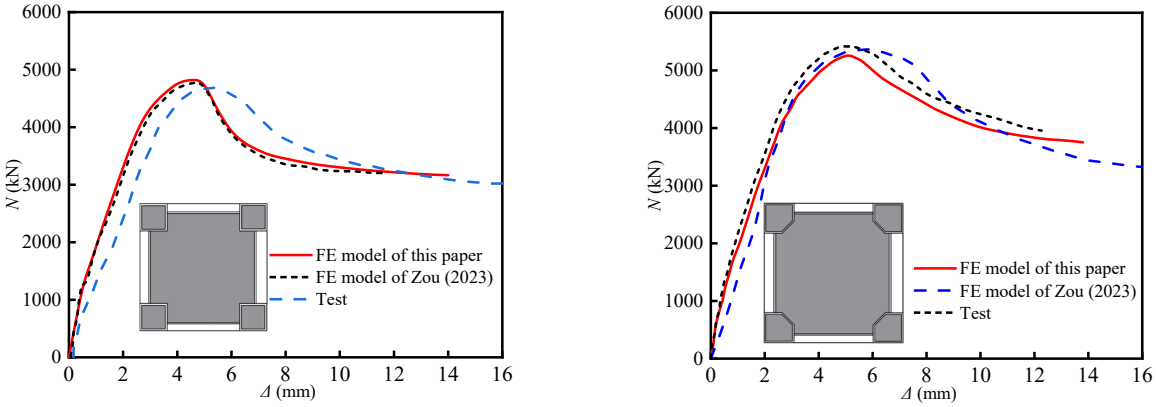
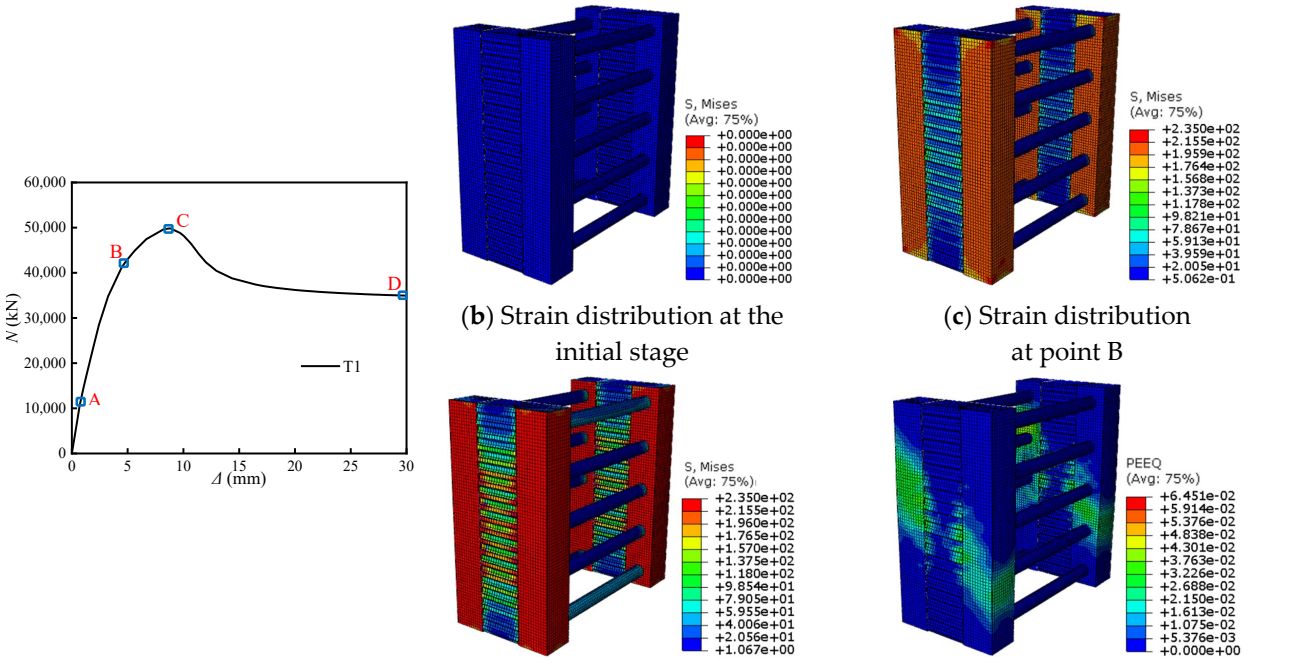


Figure 9. Comparison of load–displacement curves between test and FE model. (**a**) ST-75-75 [30]. (**b**) PST-75-45 [30].

4. Results and Analysis

4.1. Failure Modes and Phenomenon

Taking the typical specimen T1 as an example, the stress process under axial compression load can be divided into four stages: the elastic stage, the elastic–plastic stage, the plastic deformation stage, and the bearing capacity decline stage. As shown in Figure 10, the load–displacement curve and the corresponding strain–deformation diagram extracted from the FE model of specimen T1 are presented.



(**a**) *N*–axial strain of T1 (**b**) Strain distribution at the initial stage (**c**) Strain distribution at point B (**d**) Strain distribution at point C (**e**) Equivalent plastic strain of point D

Figure 10. Strain distribution during loading process of specimen T1.

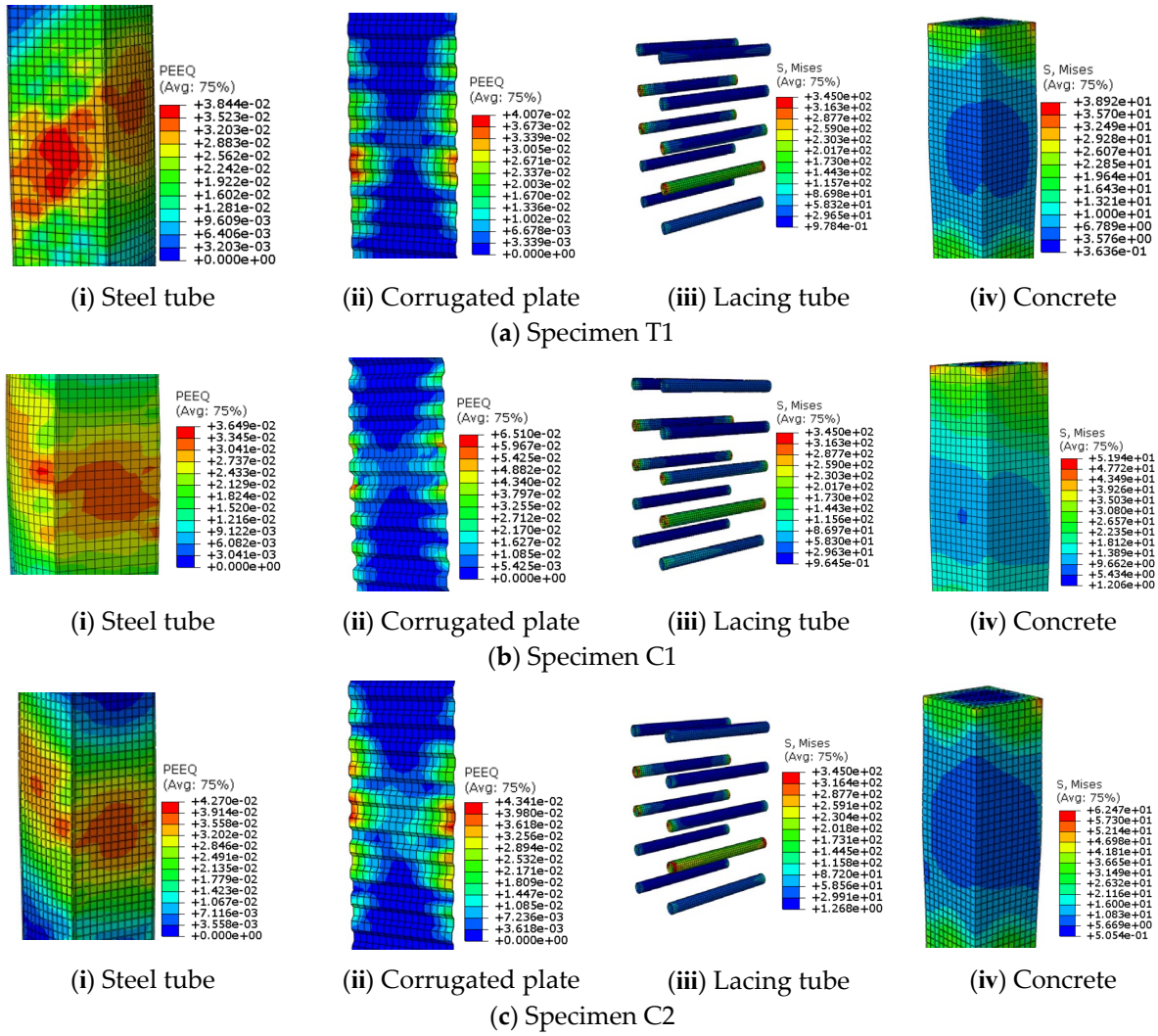
Before point A, the specimen remains in the elastic stage, exhibiting consistent overall performance. During this phase, there is a linear relationship between the axial bearing capacity and the longitudinal deformation of the component. As the strain increases and reaches point A, deformation begins at the top of CFST, accompanied by slight buckling in the local area at the top of tube. The strain in the concrete gradually increases from the center of the column to the periphery until point B, at which the load reaches 85% to 90% of the peak load, and the specimen transitions into the elastoplastic stage, characterized by a nonlinear material response. After point B, the stress within the specimen continues to rise, the stress in the concrete increases, while the stress in the steel tube expands from the center of the column outward. Notably, the stress in the middle of the corrugated steel plate and the steel tube also rises significantly. During this stage, the axial stiffness of the column gradually decreases, and the rate of load increment begins to slow down until reaching point C, marking the onset of the plastic deformation stage of the specimen, this stage BC is the plastic stage. After reaching point C, the stress within the specimen continues to increase, spreading from the column to the surrounding areas. The bearing capacity gradually declines until the loading is completed, ultimately resulting in the formation of a distinct oblique plastic strain band at point D. This indicates significant plastic deformation and marks the transition into the failure phase of the specimen.

4.2. Parameter Analysis

4.2.1. Compressive Strength of Concrete

The deformation of each specimen with a varying compressive strength of concrete is illustrated in Figure 11. Under the action of axial compression load, local buckling deformation occurs in the middle of the steel tube, and with the increase in concrete compressive strength, the equivalent plastic strain of the same position of the steel tube also increases and the obvious degree of local deformation gradually increases. The range of plastic deformation in the corrugated steel plate expands. For specimens T1 and C1, with concrete strengths of C30 and C40, respectively, the corrugated steel plate exhibits significant plastic strain at the connection between the column and the steel tube. However, for specimen C2, which has a higher concrete strength of C50, the plastic deformation of corrugated steel plate increases notably, resulting in a distinct "X"-shaped shear deformation.

Table 2 shows the relevant parameters of the axial compression performance obtained by numerical simulations for each specimen, including the peak load (Np), axial stiffness (K), and ductility coefficient (μ) under axial compression load. As illustrated in Figure 12a, the load–displacement curves for specimens with varying concrete strengths under axial compression are shown. It is evident that with the increase in concrete strength, the axial compression bearing capacity of the column gradually increases. According to Table 2, compared to the specimens with C30 concrete, specimens with C40 and C50 concrete demonstrate an increase in bearing capacity of 20% and 35%, respectively. This indicates that increasing concrete strength can effectively improve the bearing capacity of the specimens. Notably, specimen C1, with a concrete strength of C40, exhibits the highest ductility, and its ductility coefficient is 1.46 times that of the typical specimen T1. This finding suggests that the synergistic deformation capabilities of C40 concrete and Q235 steel significantly enhance the ductility of the specimen. Furthermore, as the concrete strength increases, the axial stiffness of the specimens also rises progressively, and the axial stiffness of specimen C2 is 33% higher than that of specimen T1.



(**i**) Steel tube (**ii**) Corrugated plate (**iii**) Lacing tube (**iv**) Concrete

(**a**) Specimen T1

(**i**) Steel tube (**ii**) Corrugated plate (**iii**) Lacing tube (**iv**) Concrete

(**b**) Specimen C1

(**i**) Steel tube (**ii**) Corrugated plate (**iii**) Lacing tube (**iv**) Concrete

(**c**) Specimen C2

Figure 11. Failure modes of specimens with different compressive strengths of concrete.

4.2.2. Yield Strength of Steel Tube

Figure 13 illustrates the distribution of plastic strain in steel tubes with different yield strengths subjected to axial compressive loads, as determined through numerical simulation. It can be seen that plastic deformation is most pronounced in the central region of the steel tube, and this deformation spreads around. As shown in Figure 12b, as the yield strength of the steel tube increases, the bearing capacity of the specimen also increases significantly, which indicates that the bearing capacity of the column could be enhanced by appropriately increasing the yield strength of the steel tube. According to Table 3, compared to specimen T1, the peak load of specimens H1 and H2 is increased by 21% and 28%, respectively, while the ductility coefficient of specimen H1 and H2 is decreased by 11% and 5%, respectively. It indicates that increase in the yield strength of the steel tube can effectively enhance the peak bearing capacity of specimen, while simultaneously exerting a negative influence on its ductility. In the design of the specimen, the improvement of steel tube yield strength should be integrated with the cooperative working capacity of concrete to ensure that the axial bearing capacity of the specimen is improved without excessively sacrificing ductility.

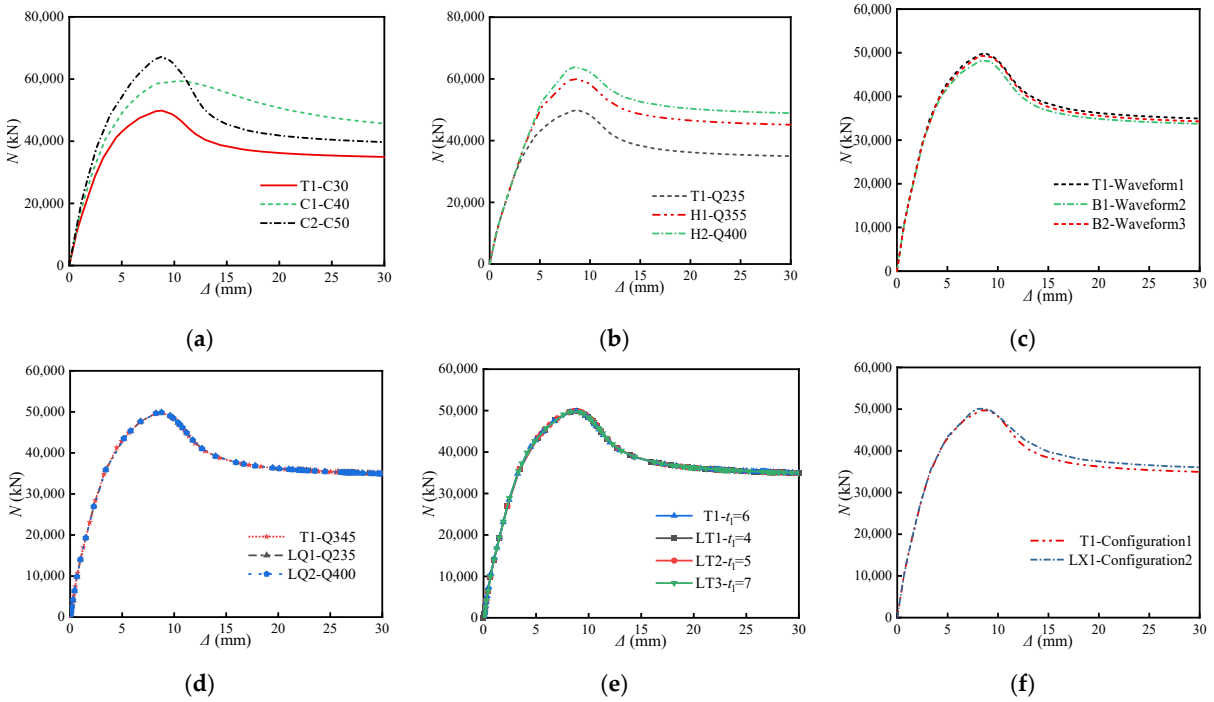


Figure 12. Load–displacement curves of specimens. (**a**) Different compressive strength of concrete; (**b**) Different yield strength of steel tube; (**c**) Different waveforms of corrugated steel plate; (**d**) Different yield strength of lacing tubes; (**e**) Different thickness of lacing tubes; (**f**) Different configuration of lacing tubes.

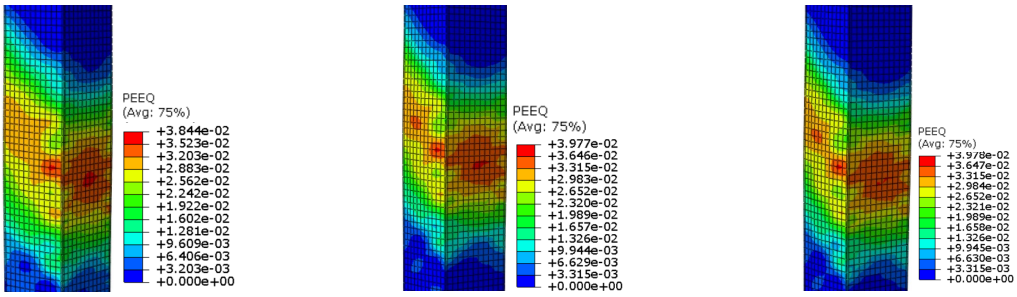


Figure 13. Equivalent plastic strain of steel tubes.

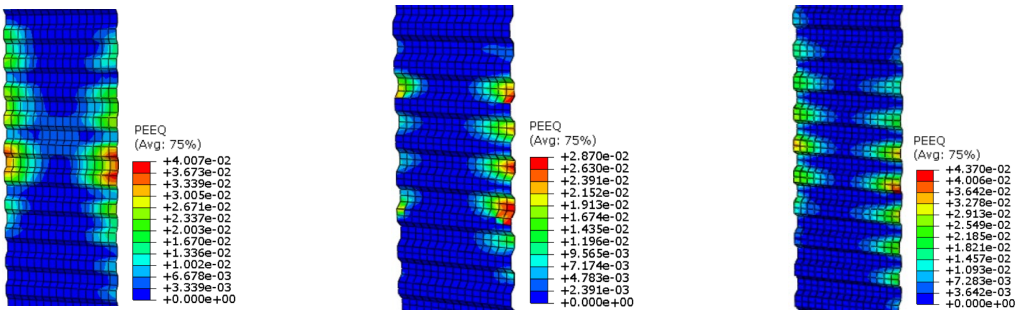
Table 3. Axial compression results of each specimen.

Specimen	Yield Strength of Steel Tube f_y (Mpa)	Compressive Strength of Concrete f_c (Mpa)	Thickness of Lacing Tubes t_l (mm)	Yield Strength of Steel Tube f_L (Mpa)	N_P (kN)	μ
T1	235	30	6	355	49,711.38	2.81
H1	355	30	6	355	60,079.23	2.51
H2	400	30	6	355	63,791.74	2.67
C1	235	40	6	355	59,422.75	4.10
C2	235	50	6	355	67,232.60	3.03
LT1	235	30	4	355	49,858.30	3.53
LT2	235	30	5	355	49,865.60	3.66
LT3	235	30	7	355	49,709.40	3.13
LQ1	235	30	6	235	44,640.10	3.57
LQ2	235	30	6	400	44,646.10	3.86
LX1	235	30	6	355	50,237.69	3.75
B1	235	30	6	355	48,234.30	2.59
B2	235	30	6	355	49,473.68	2.78

Note: N_P and μ represent the peak load and ductility coefficient of specimens, respectively.

4.2.3. Waveform of Corrugated Plate

As shown in Figure 14, the equivalent plastic strain distribution of corrugated plates with different waveforms under axial compression load is presented. When the wavelength is small (waveform 1), the plastic deformation area of the corrugated plate is larger, but the local buckling position is more concentrated, while the local buckling position of the corrugated plate with the larger wavelength (waveform 2) is larger but the plastic deformation at the center of the corrugated plate is smaller. Compared with the specimen T1 at the smallest wave height, the ductility and the axial stiffness of specimen B1 at the largest wave height are reduced by 8% and 5%, respectively, and the ductility and the axial stiffness of specimen B2 are decreased by 1% and 4%, respectively. This is due to the increase in wave height leads to a reduction in the concrete section. The bearing capacities of specimens B1 and B2 also declined compared to specimen T1. It indicates that the increase in wave height and wavelength of corrugated steel plate results in a reduction in both axial stiffness and ductility of the specimen.



(**a**) Specimen T1 (**b**) Specimen B1 (**c**) Specimen B2

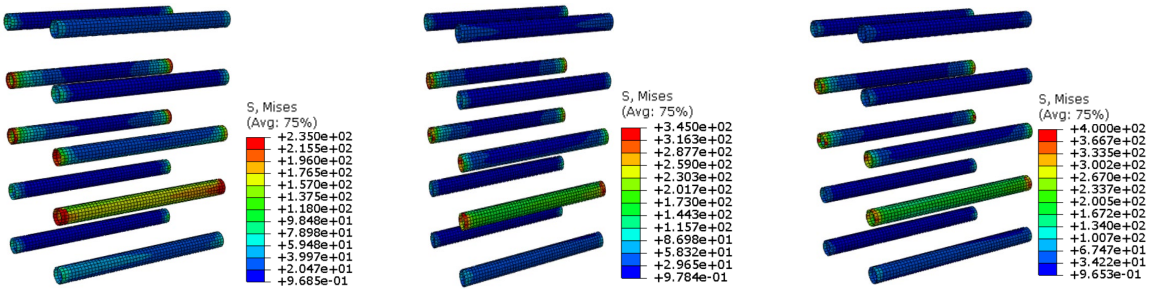
Figure 14. Equivalent plastic strain of corrugated plates.

4.2.4. Lacing Tube

As shown in Figure 15, the stress forms of lacing tubes with different yield strength are similar under axial compression load. The stress is larger in the middle and lower parts of the column, the stress is more concentrated at both ends of the lacing tube, and lower-yield-strength tubes show a larger range of stress. Figure 12d,e shows the load–displacement curves for specimens where only the strength or thickness of the lacing tube is changed. It can be seen that the thickness of the lacing tube has no obvious effect on the axial compression performance of specimens. It can be seen from Table 3 that with the increase in the thickness of the lacing tube, the ductility of the specimen decreases gradually, and the axial stiffness of the specimen T1 with Q355 lacing tube is the highest. Compared to the yield strength and thickness of the lacing tube, different configuration of lacing tube has a more significant influence on the axial compression performance of specimens. Setting diagonal tubes can enhance the axial load-bearing capacity of specimens. According to Table 3, compared with specimen T1, the bearing capacity, ductility, and axial stiffness of specimen LX1 are increased by 1%, 33%, and 12%, respectively. Therefore, diagonal lacing tubes should be considered in the design of latticed columns to enhance their axial compression performance.

In summary, compared to specimens with C30 concrete, those with C50 concrete exhibit an increase of 35% in axial bearing capacity and 33% in stiffness. The peak bearing capacity of the specimen with a steel tube yield strength of 400 MPa is 28% higher than that of the specimen with a steel tube yield strength of 235 MPa, although ductility decreases by 5%. Additionally, specimens with diagonal lacing tubes show improvements in axial bearing capacity (1%), ductility (33%), and axial stiffness (12%) compared to those with

horizontal lacing tubes. The waveform of the corrugated steel plate has minimal impact on the axial compression performance of the specimens.



(**a**) Specimen LT1 (**b**) Specimen LT2 (**c**) Specimen LT3

Figure 15. Stress distribution in lacing tubes.

Therefore, to achieve better axial compression performance in latticed columns, it is essential to appropriately increase the compressive strength of the concrete and the yield strength of the steel tube during the design process. Furthermore, the collaborative behavior between the steel tube and concrete should be carefully considered to optimize the overall bearing capacity and structural performance. The use of diagonal lacing tubes should also be prioritized in the design, as they enhance structural stability and contribute to increases in both load-bearing capacity and ductility. Finally, a careful balance between bearing capacity and ductility must be maintained to ensure the best possible structural performance.

5. Bearing Capacity Calculation Formula

According to the specification GB 50936-2014 [31], the calculation formula of the bearing capacity N_u of the axial compression member of the CFST latticed column is as follows:

$$N_u = \varphi N_0 = \varphi \sum_{i=1}^{m} A_{sc} f_{sc} \quad (1)$$

where φ is the stability coefficient; N_0 is the design value of bearing capacity and strength of axial compression members; m is the number of limbs; A_{sc} is the cross-sectional area of a single CFST limb; and f_{sc} is the design value of compressive strength of CFST limb. Therefore, the calculation formula of axial compression bearing capacity $N_{u,com}$ of the proposed latticed column is as shown in Equation (2).

$$N_{u,com} = \varphi N_{0,com} = \varphi \sum_{i=1}^{m} A_{sc,com} f_{sc,com} \quad (2)$$

where m = 2; $N_{0,com}$ represents the axial compression members' design value of bearing capacity and strength; $A_{sc,com}$ is the cross-sectional area of the composite limb (which consists of the steel tube and the corrugated steel plate filled with concrete); and $f_{sc,com}$ refers to the design value of compressive strength of the composite limb.

The concrete within the steel tube and corrugated steel plate can be regarded as confined concrete. Based on the superposition principle, without considering the influence of the slenderness ratio on the bearing capacity of composite latticed column, the calculation formula of single limb bearing capacity of latticed column $N_{0,s}$ is proposed as:

$$N_{0,s} = A_s f_s + A_{cs} f_{cs} + A_{cr} f_{cr} + A_{ccr} f_{ccr} \quad (3)$$

where A_s and f_s represent the cross-sectional area and compressive strength of square steel tube, respectively; A_{cs} and f_{cs} are the cross-sectional area and compressive strength of concrete filled in the square steel tube, respectively; A_s and f_s represent the cross-sectional area and compressive strength of corrugated steel plate, respectively; A_{ccr} is the cross-sectional area of concrete filled in the corrugated steel plate, which is averaged between the trough and peak position; and f_{ccr} is the compressive strength of concrete filled in the corrugated steel plate.

Based on numerical simulations and the existing studies [32,33], the axial compression bearing capacity of corrugated steel plate is relatively low and can be disregarded in the bearing capacity formula for the latticed column. The concrete in this study can be regarded as square steel tube confined concrete. The formulas for calculating the axial compressive strength of confined concrete are as shown:

$$f_c = f_{co,}(-1.254 + 2.254\sqrt{1 + 7.94\frac{f_r{}'}{f_{co}}} - 2\frac{f_r{}'}{f_{co}}) \tag{4}$$

$$f_r{}' = k_e f_r = 0.635 f_r \tag{5}$$

$$f_r = \frac{2t\sigma_{hp}}{D - 2t} \tag{6}$$

$$\sigma_{hp} = 0.1(D/t)^{0.5} f_{215} \tag{7}$$

where $f_r{}'$ is the effective constraint stress applied by the square steel tube to core concrete; f_r is the constraint stress from square steel tube on core concrete; k_e is the effective confinement coefficient of steel tube to core concrete; σ_{hp} represents the transverse stress of the steel tube at the peak load; f_{215} is the design strength of Q235 steel, which is 215 MPa; and D and t refer the width and thickness of the square steel tube. Thus, the calculation formulas of axial compressive strength of square steel tube filled with concrete and corrugated steel plate filled with concrete are as shown:

$$f_{cs} = f_{co,cs}(-1.254 + 2.254\sqrt{1 + 7.94\frac{f_{r,cs}{}'}{f_{co,cs}}} - 2\frac{f_{r,cs}{}'}{f_{co,cs}}) \tag{8}$$

$$f_{ccr} = f_{co,ccr}(-1.254 + 2.254\sqrt{1 + 7.94\frac{f_{r,cs}{}'}{f_{co,ccr}}} - 2\frac{f_{r,cs}{}'}{f_{co,ccr}}) \tag{9}$$

where $f_{r,cs}{}'$ is the effective constraint stress of the square steel tube to the core concrete; $f_{r,\,ccr}$ is the constraint stress of corrugated steel plate and square steel tube wall to core concrete; $f_{co,cs}$ are the axial compressive strength of square steel tube core concrete; and $f_{co,ccr}$ is the axial compressive strength of corrugated steel core concrete. According to the specification ANSI/AISC 360-05 [34], the formula for calculating the stability coefficient φ is as shown:

$$\varphi = \begin{cases} 0.658^{\lambda_n^2} & \lambda_n \le 1.5 \\ \frac{0.877}{\lambda_n^2} & \lambda_n > 1.5 \end{cases} \tag{10}$$

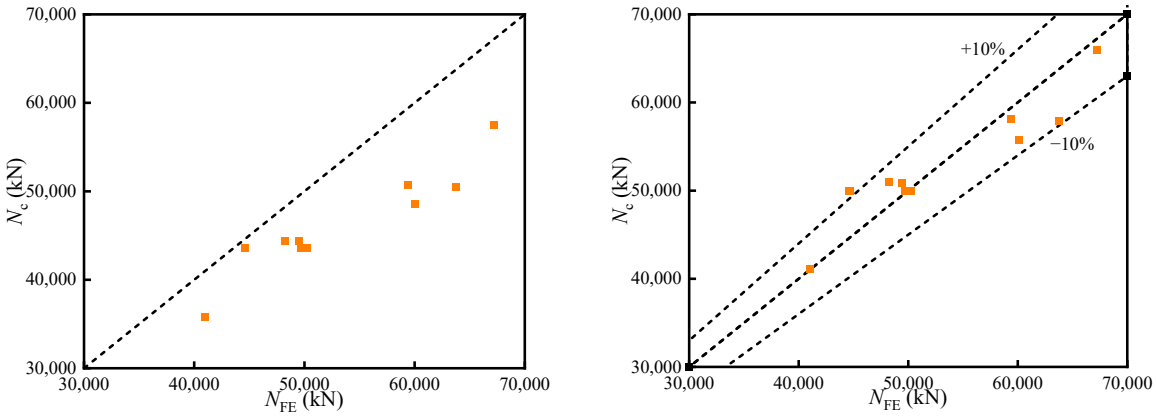
where λ_n is the relative slenderness ratio coefficient of the composite column. Therefore, the calculation formula of axial compression bearing capacity of steel tube and corrugated steel plate composite latticed column without considering the effect of batten tube is as shown:

$$N_{u,com} = 2\varphi[(A_s f_s + A_{cs} f_{cs}) + A_{cr} f_{cr} + A_{ccr} f_{ccr}] \tag{11}$$

As shown in Figure 16a, the bearing capacity of the specimens calculated according to Equation (11) without considering the axial compression contribution of the lacing

tube is compared with that obtained by numerical simulation. It can be observed that the calculated values are lower, which is attributed to the axial compression contributions from the confined concrete, steel tube, and corrugated steel plate which are considered, while the influence of the lacing tube on the axial bearing capacity of the latticed column is ignored. By linear regression, the correction coefficient α = 1.146 is determined to correct the influence of the lacing tube on the latticed column. Therefore, the calculation formula of axial compression bearing capacity of latticed column is as shown:

$$N_{u,com} = 2\alpha\varphi[(A_s f_s + A_{cs} f_{cs}) + A_{cr} f_{cr} + A_{ccr} f_{ccr}] \quad (12)$$



(**a**) Ignoring the influence of the lacing tube (**b**) Considering the influence of the lacing tube

Figure 16. Comparison of calculated values and simulated values of bearing capacity.

As seen, Table 4 and Figure 16b show the comparison between the bearing capacity calculated by Equation (12) and the bearing capacity obtained by numerical simulation in this study. The results show that the calculated value is close to the simulated value and the error is within 10%, indicating that the formulas proposed in this study have certain reference value.

Table 4. Comparison of calculation results and simulation results of specimens.

Specimen	N_c (kN)	N_{FE} (kN)	N_c/N_p
T1	49,925.40	49,711.38	1.00
H1	55,709.35	60,079.23	0.93
H2	57,878.33	63,791.74	0.91
C1	41,088.53	41,018.68	1.00
C2	58,101.43	59,422.75	0.98
C3	65,936.90	67,232.60	0.98
LT1	49,925.40	49,858.30	1.00
LT2	49,925.40	49,865.60	1.00
LT3	49,925.40	49,709.40	1.00
LQ1	49,925.40	44,640.10	1.12
LQ2	49,925.40	44,646.10	1.12
LX1	49,925.40	50,237.69	0.99
B1	50,922.60	48,234.30	1.06
B2	50,817.21	49,473.68	1.03

Note: N_c represents the theoretical calculation value of bearing capacity calculated by Formula (12); N_{FE} represents the bearing capacity obtained by numerical simulation.

6. Conclusions

To study the axial compressive mechanical properties of latticed columns with CFST tubes and corrugated steel plates, 13 composite latticed columns were designed with steel tube yield strength, concrete compressive strength, corrugated steel plate waveform, lacing tube thickness, yield strength and configuration as research parameters. The influence

of different parameters on the axial compression performance of latticed columns was analyzed. The conclusions can be drawn as follows:

(1) Increasing the compressive strength of concrete significantly enhances the axial bearing capacity and stiffness of latticed columns. Specimens with C50 concrete show a 35% higher axial bearing capacity and a 33% higher stiffness than those with C30 concrete.
(2) Compared with the specimen with a steel tube yield strength of 235 MPa, the peak bearing capacity of the specimen with a steel tube yield strength of 400 MPa increases by 28%, while ductility decreases by 5%. In the design of specimens, it is essential to balance the synergistic effects between steel strength and concrete to improve axial bearing capacity without a significant loss of ductility.
(3) Using plates with smaller wave heights and wavelengths, and incorporating diagonal lacing tubes, can enhance axial performance. Specimens with diagonal lacing tubes show a 33% increase in ductility and a 12% increase in stiffness compared to those with horizontal lacing tubes.
(4) Based on existing CFST latticed column specifications, new formulas were proposed for calculating the axial compression bearing capacity of CFST and corrugated steel plate latticed columns. The predicted values have an error within 10% compared to the simulation results.

Author Contributions: X.Z.: conceptualization, methodology, software, and writing—original draft preparation. N.Z.: supervision, formal analysis, and writing—review and editing. Z.H.: conceptualization and data curation. X.L.: funding acquisition, resources, and methodology. Y.N.: methodology and software. J.L.: data curation and software. All authors have read and agreed to the published version of the manuscript.

Funding: This research was supported by the National Natural Science Foundation of China (grant number: 52478223) and Research and Development Project of CISDI Group Co., Ltd. (grant number: 90150915-KJ-001).

Data Availability Statement: The original contributions presented in this study are included in the article. Further inquiries can be directed to the corresponding author.

Conflicts of Interest: Authors Xuan Zhao, Zhao-Hui Hu and Ying Nie was employed by the company CISDI Group Co., Ltd. The remaining authors declare that the research was conducted in the absence of any commercial or financial relationships that could be construed as a potential conflict of interest. The sponsors had no role in the design, execution, interpretation, or writing of the study.

References

1. Han, L.H. *Concrete Filled Steel Tubular Structures-Theory and Practice*; Science Press: Beijing, China, 2016.
2. Xiong, L.Z. *Study on Seismic Damage Behavior of Four-Tube Concrete Filled Steel Tubular Laced Columns*; Hunan University of Science and Technology: Changsha, China, 2023.
3. Nie, J.G.; Liao, Y.B. Axial compression test of concrete-filled steel tubular latticed columns with four limbs. *J. Tsinghua Univ. (Nat. Sci.)* **2009**, *49*, 1919–1924.
4. Chen, B.C.; Ou, Z.J. Experimental study on the ultimate load carrying capacity of four-tube concrete filled steel tubular laced columns. *China Civ. Eng. J.* **2007**, *40*, 32–41.
5. Deng, X.Y. *Study on the Seismic Performance of Concrete Filled Steel Tubular Latticed Column*; Central South University: Changsha, China, 2013.
6. Yang, Y.F.; Liu, M.; Fu, F. Experimental and numerical investigation on the performance of three-legged CFST latticed columns under lateral cyclic loadings. *Thin-Walled Struct.* **2018**, *132*, 176–194. [CrossRef]
7. Kawano, A.; Sakino, K. Seismic resistance of CFT trusses. *Eng. Struct.* **2003**, *25*, 607–619. [CrossRef]
8. Ou, Z.; Chen, B.; Hsieh, K.H.; Halling, M.W.; Barr, P.J. Experimental and analytical investigation of concrete filled steel tubular columns. *J. Struct. Eng. ASCE* **2011**, *137*, 635–645. [CrossRef]

9. Yuan, H.H.; Wu, Q.X.; Chen, B.C.; Cai, H.X. Pseudo-dynamic test of CFST latticed columns with flat lacing tubes. *Eng. Mech.* **2019**, *36*, 67–78.
10. Huang, Z.; Jiang, L.Z.; Zhou, W.B.; Chen, S. Studies on restoring force model of concrete filled steel tubular laced column to composite box-beam connections. *Steel Compos. Struct.* **2016**, *22*, 1217–1238. [CrossRef]
11. Liao, X.; Zhao, X.; Li, X.; Hu, Z.H.; Liu, J.; Nie, Y.; Chen, S.Y.; Liu, X.G. Fatigue cracking of shoulder beams and I-shaped corbels within four-limb CFST columns. *J. Constr. Steel Res.* **2024**, *220*, 108812. [CrossRef]
12. Yu, Z.; Liu, F.Q.; Lu, W.; Liu, C.Y.; Wang, Y.Y.; Wu, Z.M. Experimental study on shear behavior of tie-bar connectors in corrugated steel-concrete composite panels. *J. Build. Struct.* **2024**, *45*, 284–290.
13. Park, K.J.; Jung, K.; Kim, Y.W. Evaluation of homogenized effective properties for corrugated composite panels. *Compos. Struct.* **2016**, *140*, 644–654. [CrossRef]
14. Su, R.; Li, X.; Zhong, T.; Zhou, T. Axial behavior of novel CFDST columns with outer welded corrugated steel tubes. *Structures* **2021**, *34*, 2708–2720. [CrossRef]
15. Liao, X.; Li, X.; Zhao, S.D.; Yang, C.; Yin, D.D. Behavior of eccentrically loaded rectangular CFST components for shear walls using double horizontally-corrugated steel plates. *Eng. Struct.* **2024**, *303*, 117470. [CrossRef]
16. Liao, X.; Li, X.; Li, Z.W.; Li, C.Z.; Zhong, T. Flexural behavior of novel CFDST components with external welded corrugated steel tubes. *Structures* **2023**, *52*, 42–56. [CrossRef]
17. J'ager, B.; Dunai, L.; Kovesdi, B. Lateral-torsional buckling strength of corrugated web girders-Experimental study. *Structures* **2022**, *43*, 1275–1290. [CrossRef]
18. Shariatyazdi, P.; Ronagh, H.; Izadinia, M.; Javaheritafti, M.R. Shear buckling behavior of tapered cantilever beams with corrugated trapezoidal web under concentrated tip load. *J. Constr. Steel Res.* **2022**, *193*, 107265. [CrossRef]
19. Alikhanifard, M.A.; Rahai, A.R.; Tehrani, P. A new shear strength model for steel corrugated web girders. *J. Constr. Steel Res.* **2022**, *197*, 107457. [CrossRef]
20. Changyu, W.; Shiping, Y.; Boxue, W.; Jianhua, D.; Xiaoping, R.; Xiaoliang, Z. Research on the transverse flexural performance of T-PBL joints between corrugated steel webs and concrete slabs. *Structures* **2022**, *44*, 1057–1069. [CrossRef]
21. Zhang, Z.; Li, G.Q.; Sun, F.F. Flexural behavior of the composite beam with corrugated webs. *China Civ. Eng. J.* **2014**, *47*, 34–39.
22. Liu, Z.F.; Wang, Z.Y.; Zhou, X.F. Bending behavior of composite girders with corrugated steel webs and concrete filled steel tube flanges. *J. Build. Struct.* **2019**, *40*, 325–332.
23. Wang, J.X.; Zhang, N.N.; Gao, S. Numerical study on the anti-impact performance of novel concrete-filled steel tubular joint with corrugated web and cover plates. *J. Constr. Steel Res.* **2023**, *211*, 108168. [CrossRef]
24. Feng, J.S.; Sun, Z.X.; Zou, Y.; Wang, C.Q. Finite element analysis of axial compression performance of steel tube-corrugated steel plate confined concrete composite column. *Steel Constr. (Chin. Engl.)* **2023**, *38*, 14–21.
25. Sokołowski, D.; Kami´nski, M. Stochastic Reliability-Based Design Optimization Framework for the Steel Plate Girder with Corrugated Web Subjected to Corrosion. *Materials* **2022**, *15*, 7170. [CrossRef]
26. Lai, Y.; Zhang, Y.J.; Liu, L.; Wei, X.; Fang, E.; Lua, J. Integrating CAD with Abaqus: A practical isogeometric analysis software platform for industrial applications. *Comput. Math. Appl.* **2017**, *74*, 1648–1660. [CrossRef]
27. Esmaeily, A.; Xiao, Y. Behavior of reinforced concrete columns under variable axial loads: Analysis. *ACI Struct J.* **2005**, *102*, 736–744.
28. Yu, H.L.; Jeong, D.Y. Application of a stress triaxiality dependent fracture criterion in the finite element analysis of unnotched Charpy specimens. *Theor. Appl. Fract. Mech.* **2010**, *54*, 54–62. [CrossRef]
29. Bao, Y.B.; Wierzbicki, T. On fracture locus in the equivalent strain and stress triaxiality space. *Int. J. Mech. Sci.* **2004**, *46*, 81–98. [CrossRef]
30. Zou, Y.; Wang, L.; Sun, Z.; Pan, J.; Chen, M.; Wu, Y. Experimental and numerical studies of concrete-filled corrugated steel tubular column under axial compression. *Eng. Struct.* **2023**, *276*, 114813. [CrossRef]
31. *GB 50936-2014*; Technical Code for Concrete Filled Steel Tubular Structures. China Building Industry Press: Beijing, China, 2014.
32. Mander, J.B.; Priestley, M.J.; Park, R. Theoretical stress-strain model for confined concrete. *J. Struct. Eng.* **1988**, *114*, 1804–1823. [CrossRef]
33. Zhou, X.H.; Gan, D.; Liu, J.P.; Zhang, S. Experiment and analysis on square tubed rein forced concrete stub columns under axial compression. *J. Build. Struct.* **2011**, *32*, 68–74.
34. *ANSI/AISC 360-05*; Specification for Structural Steel Buildings. American Institute of Steel Construction: Chicago, IL, USA, 2005.

Disclaimer/Publisher's Note: The statements, opinions and data contained in all publications are solely those of the individual author(s) and contributor(s) and not of MDPI and/or the editor(s). MDPI and/or the editor(s) disclaim responsibility for any injury to people or property resulting from any ideas, methods, instructions or products referred to in the content.